

Capturing the drag crisis in the flow around a smooth cylinder using a hybrid RANS-LES model on coarse meshes

Michael D. Mays^{a,*}, Sylvain Lardeau^b, Sylvain Laizet^a

^a Department of Aeronautics, Imperial College London, Exhibition Road, South Kensington, London, SW7 2BX, UK

^b Siemens Digital Industry Software GmbH, Nuremberg, Germany

ARTICLE INFO

Keywords:

Hybrid RANS-LES

Drag crisis

Critical and super-critical

ABSTRACT

A hybrid strategy combining Reynolds-averaged Navier–Stokes (RANS) and large eddy simulation (LES) methods is nowadays seen as an efficient way to simulate turbulent flows of practical relevance. In this work, the scale-resolving hybrid (SRH) model proposed by Manceau (2018) is compared with a conventional unsteady RANS model, and LES and experimental data from the literature for the flow around a smooth cylinder in the flow regime around the drag crisis. Based on a temporal filtering formalism, this approach has seen limited testing for turbulent separated flows. The drag crisis phenomenon is dominated by complex near-wall physics and is challenging to simulate. The predictive accuracy and the robustness to mesh coarsening for the SRH model are assessed for this test case, with the aim to demonstrate that this hybrid approach can be a credible cost-saving alternative to LES for separated turbulent flows. The meshes considered in this numerical study are far coarser than the ones used in the LES reference data, yet, the results for the time mean drag are found in good agreement with the reference data. Other features of the flow, such as the presence and sizes of the laminar separation bubbles and the consequent magnitude of the time mean lift are not as well captured. In general, the qualitative behaviour of the SRH model is good when considered in the context of questions previously raised in the literature about hybrid models. The mesh savings are achieved by coarsening the spatial resolution in the wake, whereas the resolution required in the near-wall area and shear layers remains high, though much reduced compared to the reference LES data. The key point taken from this study is that the SRH model is an attractive option to produce higher-fidelity data on coarse meshes.

1. Introduction

While the Navier–Stokes equations constitute a broadly accepted mathematical model to describe the motions of a turbulent flow, their solutions can be extremely challenging to obtain due to the chaotic and inherently multi-scale nature of turbulence. The smallest scales impact the largest scales, and small changes to boundary conditions, initial conditions, or mesh resolution, for example, can have a dramatic impact on the solution. A particular challenge is the non-linear cascade of turbulent energy from large eddy scales to the small dissipation scales, at which turbulent energy is converted to heat. The turbulent scales are typically separated by many orders of magnitude. A simulation that resolves all of these scales is called direct numerical simulation (DNS). Except for the simplest of problems, simulating turbulent flows require high-performance computing (HPC). However, even with today's state-of-the-art algorithms, codes, and petascale computing systems, DNS is only feasible for a small class of problems, namely those at moderate Reynolds numbers (defined as the ratio of inertial forces to viscous forces) and in simple geometries.

One strategy to address this issue is to reduce the computational cost of simulations by introducing a certain level of modelling of the turbulence, leading to the design of Reynolds-averaged Navier–Stokes (RANS) and large eddy simulation (LES) equations. Ideally, LES, for which most of the turbulence scales are resolved while only the smallest scales are modelled, is preferable, but this strategy can still be computationally extremely expensive (almost as expensive as DNS), especially for wall-bounded turbulent flows. RANS approaches are based on a statistical treatment of the Navier–Stokes equations which are then solved to provide average quantities, with a model for the correlations which appear when averaging the non-linear terms of the governing equations. The small turbulent scales are not present in RANS approaches and as a result, the computational cost and mesh requirement are more manageable than for DNS/LES, especially for turbulent flows of practical relevance. Unfortunately, the generality and the predictive potential of RANS approaches is consequently limited, in particular for separated flows.

* Corresponding author.

E-mail address: mdm114@ic.ac.uk (M.D. Mays).

<https://doi.org/10.1016/j.ijheatfluidflow.2023.109203>

Received 15 February 2023; Received in revised form 14 June 2023; Accepted 17 July 2023

Available online 19 August 2023

0142-727X/© 2023 The Author(s). Published by Elsevier Inc. This is an open access article under the CC BY license (<http://creativecommons.org/licenses/by/4.0/>).

This has prompted the development of alternative simulation strategies, such as hybrid RANS/LES methods, which introduce alterations to a RANS model such that unsteady RANS (URANS) is utilised close to walls (boundary layers) while LES is used elsewhere (Spalart et al., 1997; Girimaji, 2006). Such hybrid approaches are known to be difficult to implement, due to the fundamental inconsistency between RANS and LES: LES have turbulent fluctuations, whereas RANS approaches are not designed to deal with these fluctuations. There are also issues regarding mesh requirement and significant questions remain about the promise of hybrid RANS/LES models to simulate complex flow fields at reduced computational cost without a substantial loss in accuracy, particularly for highly-separated flows. There are also concerns with the near wall behaviour of hybrid models, including how to deal with the transition between the RANS-mode and LES-mode (grey-area effects). The reviews of hybrid RANS/LES methods by Heinz (2020) and Chaouat (2017) has identified key areas of concern for hybrid methods and ideal formulations. In particular, the review of Heinz (2020) highlighted the importance of the mechanism by which the model responds to the resolved content via the mesh size and the particular method by which the resolved content is determined.

The motivation of this study is to assess the ability, robustness and behaviour of a novel hybrid model by attempting to capture the main features of the flow around a smooth cylinder for Reynolds numbers in the critical and supercritical regimes, such as the separation behaviour, onset and development of the mechanisms underlying the break-down of the shear-layer and production of vortex shedding. The scale-resolving hybrid (SRH) model proposed by Duffal et al. (2019), which operates in the same basic manner as other hybrid RANS/LES methods including Delayed Detached Eddy Simulation (DDES) model (Gritskevich et al., 2012), is compared with the underlying three-equation URANS model for various mesh resolutions. As with DDES, the SRH model introduces an altered destruction term of the sub-filter turbulent kinetic energy transport equation, in this case using a variable ψ_H , the SRH correction factor. The major difference between the two models is the different ways to determine this correction factor and its sensitivity to the amount of resolved turbulent kinetic energy. By working on the basic assumption of time filtering the Navier–Stokes equations, as opposed to the usual spatial filtering of LES, the SRH model produces a theoretically unified model smoothly transitioning from RANS to LES behaviour — this is given that the increasing filter width of a time scale filter theoretically tends to the RANS equations in the limit. For practical purposes this is amended through the use of a shielding function intended to prevent transition to LES mode by the model in the near wall region which does not have sufficient spatial resolution to sustain it.

The case of the turbulent flow around a smooth cylinder at different Reynolds numbers around the drag crisis presents an excellent test for numerical modelling research. The capacity to accurately simulate this case is significant both for its application to the ubiquitous real-world specific case of circular structures in cross-flow, but also as a case representative of separated flow where the separation point is not enforced by the geometry. Therefore, despite the symmetric configuration of the geometry and the simplicity of the case conditions, prediction of the precise separation point and the free shear layer breakdown presents a substantial challenge for turbulence closure models and numerical schemes. This difficulty is compounded for hybrid methods due to the RANS-to-LES transition in the vicinity of the wall, co-located in this case with the area of separation and free shear layers.

The flows in this study are in the critical and super-critical regimes meaning that the transition to turbulence takes place in one or more of the boundary layers immediately after laminar separation, which then rapidly reattaches to the cylinder. Consequently, the flow stays attached to the cylinder surface longer leading to a significant reduction in the drag coefficient, a phenomenon referred to as the drag crisis, illustrated by the results in Fig. 1. The drag coefficient drops to approximately 0.2 (Zdravkovich, 1997) over the course of the critical regime,

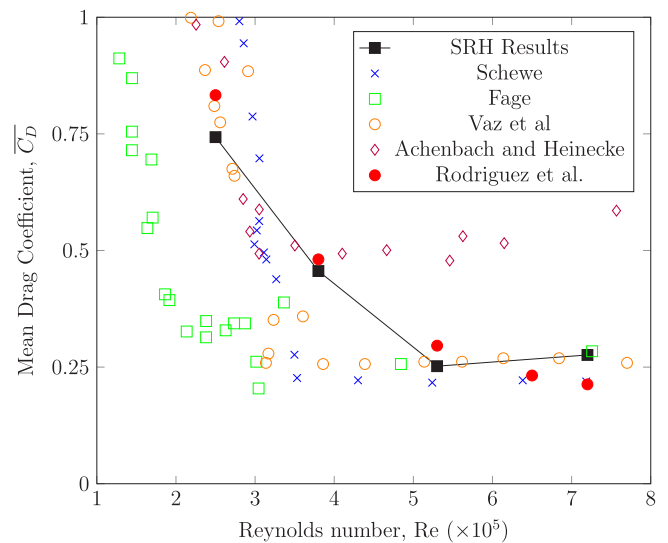


Fig. 1. Time-mean drag coefficient for critical to super-critical Reynolds numbers with reference LES data from Rodríguez et al. (2015) and experimental data from Schewe (1983), Fage (1930), Vaz et al. (2007), Achenbach and Heinecke (1981). Present results are highlighted with black squares.

afterwards stabilising to a value of 0.24 according to Rodríguez et al. (2015) as the flow moves into the super-critical regime. The critical regime also sees an initial disruption of the vortex shedding, with no clear Strouhal number in the middle band of the regime, and a mean lift coefficient an order of magnitude larger than at lower Reynolds numbers, before the smooth shedding is restored (Rodríguez et al., 2015) at a higher Strouhal number of approximately 0.44.

The effectiveness of turbulence models in accurately depicting turbulent flows where the transition happens within the free shear layer hinges on four crucial physical aspects: the initiation of the Kelvin–Helmholtz instability in the free shear layer, the spread of the Kelvin–Helmholtz vortices over space, the descent into turbulence, and the roll-up and shedding of vortices in the turbulent free shear layer. The presence of these phenomena is contingent upon the Reynolds number. As the Reynolds number rises, the starting point of instabilities within the free shear layer moves upstream towards the cylinder, resulting in a more expeditious spread of the Kelvin–Helmholtz vortices. Consequently, the simulation results become increasingly sensitive to the turbulence closure model’s performance near the wall. A detailed discussion of the physics involved in this case and the other regimes of vortex shedding can be found in Zdravkovich (1997). In the particular example of the critical and super-critical regimes important characteristics have been identified through numerical and experimental studies. The numerical study from Lehmkuhl et al. (2014) used the Wall-Adapting Local-Eddy viscosity (WALE) LES model (Nicoud and Ducros, 1999) on fine meshes to capture the drag crisis. Importantly, three different flow configurations were observed around the drag crisis: one-bubble asymmetric mode, where a laminar separation bubble is present on one side of the cylinder only; two-bubble asymmetric mode with two bubbles but with slightly different sizes producing asymmetry in the overall flow and a two-bubble symmetric mode on entering into the super-critical regime.

The importance of the flow over a smooth cylinder to industrial applications and as academic test case has motivated an extensive number of numerical studies (Breuer, 2000; Moussaed et al., 2014; Rodríguez et al., 2015; Palkin et al., 2016; Pereira et al., 2018, 2019) to investigate the flow physics and to assess the performance of turbulence models in simulating such separated flows. An early numerical study from Breuer (2000) considered the flow around a smooth cylinder conducted at a Reynolds number of 140,000. The author investigated

the influence of LES sub-grid scale modelling (SGS) and mesh resolution on the quality of the predicted results. The simulations were performed on various meshes with the Smagorinsky (Smagorinsky, 1963) and the dynamic sub-grid scale (Germano et al., 1991) models. Overall, these LES results agreed fairly well with the experimental reference data, especially in the near wake. Discrepancies were reported in the far wake with a strong dependence on the mesh resolution. Further investigations of purely LES methods applied to the flow around a smooth cylinder around the drag crisis were conducted in Rodríguez et al. (2015). The authors looked at the characteristic length scales of the wake in the critical and super-critical regimes and discussed the periodic nature of the flow by means of unsteady drag and lift loads. The power spectra of the unsteady lift showed a narrow band peak for all Reynolds numbers under scrutiny except $Re = 3.8 \times 10^5$, while the plateau behaviour of the wake parameters was observed in the super-critical regime.

Investigation of the drag crisis has also prompted a substantial number of experimental studies, producing a large amount of data albeit with a significant spread in results. The bulk of these studies have focused on the mean force coefficients with Schmidt (1965) and Fung (1960) providing additional data on the fluctuations in the forces. The authors in Achenbach and Heinecke (1981) and Schewe (1983) give values for the Strouhal number across the critical regime but each providing entirely different sets of behaviour. Given the variation in experimental results as seen in Fig. 1, the primary point of comparison for this work will be with the numerical results of Rodríguez et al. (2015). In this study, the authors made a detailed consideration of their results in relation to the spectrum of available experimental data and of the quality of the experimental data in general.

The paper is organised as follow. Section 2 lays out the numerical methodology used throughout this numerical study. Section 3 then discusses the results of the study looking in particular at the forces and their fluctuations, as well as some topological features of the flow, comparing with previous numerical studies and experiment where possible. Subsequently, the focus is placed on the behaviour of the hybrid model, especially in comparison with its URANS counterpart and reference LES, and on considerations of resolution requirements with respect to the potential for the hybrid method to provide computational savings relative to more resolving methods. Finally, Section 4 considers the main conclusions of the study with a discussion for further steps and points of future interest.

2. Methodology

The simulations in this numerical study are performed with Simcenter STAR-CCM+ (version 2022.1). It is a multi-physics computational fluid dynamics (CFD) software, based on a segregated finite volume method to solve the time-dependent governing flow equations for incompressible turbulent flow (Siemens, 2021).

2.1. Turbulence model

The RANS model used for the URANS simulations and as the basis for the SRH model is the Lag Elliptic Blending (EB) $k-\epsilon$ model derived by Lardeau and Billard (2016). In addition to solving transport equations for the turbulent kinetic energy, k , and the turbulent dissipation rate, ϵ , it solves an additional transport equation based on the lag between the stress and strain to better account for transition and non-linear behaviours. Preliminary studies (Mays et al., 2021) showed that this model was the most appropriate of the available for this instance of separated flow around a bluff body. Further simulations for comparison were conducted using the WALE model (Nicoud and Ducros, 1999).

2.1.1. Lag Elliptic Blending (EB) $k-\epsilon$ RANS model

The incompressible RANS equations can be expressed as:

$$\frac{\partial U_i}{\partial x_i} = 0 \quad (1)$$

$$\frac{\partial U_i}{\partial t} + \frac{\partial U_i U_j}{\partial x_j} = \frac{1}{\rho} \frac{\partial P}{\partial x_i} + \nu \frac{\partial^2 U_i}{\partial x_i \partial x_j} + \frac{\partial T_{ij}}{\partial x_j} \quad (2)$$

where x_i is the i component of position in 3D space and t the time. U_i , P and ρ represent the mean velocity i -component, mean pressure and density respectively and ν is the kinematic viscosity. The Boussinesq approximation for the closure is used for the Reynolds stress tensor, T_{ij}

$$T_{ij} = 2\nu_t \bar{S}_{ij} - \frac{1}{3} k \delta_{ij} \quad (3)$$

where \bar{S}_{ij} is the mean-strain-rate tensor and δ_{ij} is the Kronecker delta. The turbulent viscosity, ν_t , is determined using the typical method except for the introduction of the reduced stress function ϕ

$$\nu_t = C_\mu \phi \frac{k^2}{\epsilon} \quad (4)$$

which acts to reduce the viscosity usually over-predicted by failing to account for the lag between the stress and strain (Lardeau and Billard, 2016). The Lag EB iteration improves on the basic EB $k-\epsilon$ model (Billard and Laurence, 2012) by reconstructing the transport equation for ϕ by analogy with a Reynolds Stress Model (RSM) which produces a sensitivity to transition and non-linear effects.

The Lag EB equation system consists of three transport equations, the usual k and ϵ equations with a transport equation for the reduced stress function ϕ , and an elliptic blending function besides

$$\frac{Dk}{Dt} = \nabla \cdot \left[\left(\frac{\nu}{2} + \frac{\nu_t}{\sigma_k} \right) \nabla k \right] + P_k - \epsilon \quad (5)$$

$$\frac{D\epsilon}{Dt} = \nabla \cdot \left[\left(\frac{\nu}{2} + \frac{\nu_t}{\sigma_\epsilon} \right) \nabla \epsilon \right] + \frac{\epsilon}{k} C_{\epsilon 1} P_\epsilon - C_{\epsilon 2} \frac{\epsilon^2}{k} \quad (6)$$

$$\frac{D\phi}{Dt} = \nabla \cdot \left[\left(\frac{\nu}{2} + \frac{\nu_t}{\sigma_\phi} \right) \nabla \phi \right] + P_\phi \quad (7)$$

$$\nabla \cdot (L^2 \nabla \alpha) = \alpha - 1 \quad (8)$$

where $\sigma_k, \sigma_\epsilon, \sigma_\phi$ are diffusive constants of fixed value, $P_k = \nu_t S^2$ is the turbulent kinetic energy production and P_ϵ is the production of the turbulent dissipation rate. The alpha parameter solved for by the elliptic equation models the wall blockage and other elliptical effects and feeds into the P_ϕ term. The full expressions for the production terms P_ϕ is very lengthy and therefore is given in the appendix. The $L = k^{3/2}/\epsilon$ term in the elliptic blending is a length scale representing the integral scales.

2.1.2. Scale-resolving hybrid (SRH) model

The SRH model proposed by Duffal et al. (2019) functions on a similar basis to other hybrid RANS/LES models, which operates by modifying a URANS model by introducing an alteration into the dissipation term of the turbulent kinetic energy to promote dissipation. Likewise, the SRH model alters the turbulent kinetic energy transport equation by introducing a multiplicative factor ψ_H to the dissipation term

$$\frac{\partial(\rho k_{sfs})}{\partial t} + \frac{\partial(\rho k_{sfs} U_i)}{\partial x_i} = \frac{\partial}{\partial x_j} \left[\left(\frac{\mu}{2} + \frac{\mu_t}{\sigma_{k_{sfs}}} \right) \frac{\partial k_{sfs}}{\partial x_j} \right] + 2\mu_t S^2 - \psi_H \rho \epsilon_{sfs} \quad (9)$$

where $\mu_t = \rho \nu_t$ is the eddy diffusivity and S is the modulus of strain rate tensor. All other quantities are determined in the same way as for the RANS method, only now they represent sub-filter scale versions of their RANS equivalents (as indicated by the sfs subscript).

The ψ_H function is formulated in such a way that it always has a value greater than 1. By taking a value higher than 1 and enhancing

the dissipation of the modelled turbulent kinetic energy (here written as k_{sfs} for 'sub-filter scale' turbulent kinetic energy), k_{sfs} is reduced and the sub-grid viscosity likewise, the equation for which is Eq. (4) but with sub-filter scale quantities rather than time mean equivalents. This correction factor is derived by formally assuming that a temporal filtering procedure is applied to the Navier–Stokes equations, yielding

$$\psi_H = 1 - f_s + f_s \frac{1}{r_K} \left(\frac{4}{3} - \frac{1}{3} r_K^{3/4} \right) \frac{k_{sfs}}{k_t} \quad (10)$$

where f_s is a shielding function to force URANS behaviour in the near-wall, k_{sfs} is the instantaneous value of the modelled turbulent kinetic energy and $k_t = k_m + k_r$ is the time-mean total turbulent kinetic energy, where k_m and k_r are the time-averaged values of modelled and resolved turbulent kinetic energy respectively. The SRH Energy Ratio, r_K is a theoretically predicted ratio of modelled-to-total turbulent kinetic energy that should be attainable at a point in the mesh given a certain cell size and time step

$$r_K = 1 - \max(0, 1 - \beta_\psi \text{CFL}_H^{2/3}) \quad (11)$$

where $\beta_\psi = 0.69$ as determined by calibration using isotropic decaying turbulence and is assumed constant for all flow conditions. CFL_H represents a theoretical CFL number for the filtered quantities

$$\text{CFL}_H = \frac{\epsilon}{k_t^{3/2}} \max(\Delta t U_s, \Delta) \quad (12)$$

where Δ is the cube-root of the cell volume, $U_s = \|U\| + \sqrt{k_t}$ is a sweeping velocity giving a mean velocity value that includes the effect of turbulent motion.

Consideration will be made in this study to whether the theoretical ratio r_K , which is used to drive the hybridisation, matches the observed ratio in the simulations. The presence of the mean resolved kinetic energy in Eq. (10) is significant as it is an indicator of the level of resolved content for the hybrid model which can modify the level of modelled content in response, a key feature as identified by Heinz (2020), and a major difference from DES formulations.

The shielding function present in Eq. (10) is designed to enforce a RANS behaviour in the near-wall regions where the mesh resolution is not sufficient to sustain an LES behaviour but, under ambiguous conditions, the model tries to do so regardless. The shielding function is derived using a calibrated ratio between the wall distance, d , and the Kolmogorov length scale giving

$$f_s = 1 - \tanh \left[45 \left(\frac{v^{3/4}}{\epsilon^{1/4} d} \right)^8 \right] \quad (13)$$

The exact formulations and numerical treatments of these models may be found in the Simcenter STAR-CCM+ documentation (Siemens, 2021). As a general point all the SRH time-averaged quantities required for the model. e.g. k_t , k_r , are calculated using an exponentially-weighted averaging method over 300 time-steps (the number of time-steps is fixed by STAR-CCM+).

Given the low y^+ value, the 'All Y^+ wall treatment' option in STAR-CCM+ was used (though the 'Low Y^+ option would be equally appropriate). This is the most flexible option which at low y^+ values leads to explicit resolution of the near-wall region for the velocity and the application of the usual wall functions applicable to the viscous layer for the turbulent dissipation rate and the production of turbulent kinetic energy.

2.2. Discretisation and temporal schemes

The discretisation scheme applied to the convective terms in the SRH simulations is the Hybrid-Bounded Central Differencing (Hybrid-BCD) which blends smoothly between a second-order upwinding scheme and a bounded central difference scheme where the flux of quantity ϕ at the cell face can be expressed as

$$(\dot{m}\phi)_f = \dot{m}(\sigma_{HU}\phi_{SOU} + (1 - \sigma_{HU})\phi_{BCD}), \quad (14)$$

Table 1

Mesh prism-layer parameters used for simulations. N_r , N_θ , N_z , number of cells in the prism layer grid in the radial and azimuthal directions; L_z , spanwise domain length; Δr_1 , prism layer first cell thickness.

Mesh	N_r	N_θ	N_z	L_z/D	$\Delta r_1/D$	$\Delta t * U_\infty/D$
A	50	600	94	1.6	3.0×10^{-5}	1.0×10^{-3}
B	55	650	94	1.6	2.0×10^{-5}	7.5×10^{-4}
C	65	700	72	1.0	1.5×10^{-5}	7.5×10^{-4}
D	70	750	72	1.0	1.0×10^{-6}	5.0×10^{-4}

where \dot{m} is the mass flow rate. ϕ_{SOU} and ϕ_{BCD} are the gradients of ϕ as determined by second order upwinding and bounded central difference methods respectively and σ_{HU} is the blending parameter, here equal to the SRH shielding function given in Eq. (13). This choice was made to ensure that the scheme acts as an upwinding scheme in the enforced RANS zones while transitioning to a centred scheme in LES-like zones.

If a cell fails the boundedness criterion it reverts to a first order upwinding scheme. The following bounding provides a stable and robust behaviour

$$(\dot{m}\phi_{BCD})_f = \begin{cases} \dot{m}\phi_{FOU} & \text{if unbounded} \\ \dot{m}(\sigma\phi_{BCD} + (1 - \sigma)\phi_{SOU}) & \text{if bounded.} \end{cases} \quad (15)$$

Here, σ is a user-defined parameter introducing some upwinding in the bounded case for stability and robustness. For all the simulations in this study $\sigma = 0.01$ was chosen after a preliminary investigation, in order to eliminate checkerboarding upstream of the cylinder without negatively impacting the energy conserving effects of the centred scheme. For the URANS simulations the conventional second order upwinding scheme is used.

The time integration is achieved with a backward second order implicit time integration scheme, with the number of inner iterations fixed at 3, deemed acceptable as a low Courant number is achieved throughout while limiting the computational cost of the simulations (and test simulations with 4 inner iterations showed very little difference). A small time-step, in line with previous studies, is chosen throughout to prevent issues with inadvertent filtering of the field. This choice of time step yields a time-averaged convective Courant number of less than 2 for all the cases. The diffusion term is discretised using a second order central difference scheme.

2.3. Domain and mesh resolution

The simulations are conducted on an unstructured mesh with a blend of prism layer cells around the cylinder and triangular prisms throughout the rest of the domain. The square domain, seen in Fig. 2 (left) is $20D \times 20D$ with a Cartesian coordinate system (x, y, z) with origin at the centre of the cylinder of diameter D , located $5D$ in from the inlet. This gives a blockage ratio of 5% which should have negligible effect on the results (Zdravkovich, 1997).

The spanwise length L_z varies between the meshes, with the values shown in Table 1. This length was chosen to ensure that the largest structures can be captured in line with the fluctuation correlation studies in Rodríguez et al. (2015). The consequent aspect ratios for the simulations are 1 and 1.6. While the choice of aspect ratio can have a substantial effect on experimental results, numerical studies have shown little effect at high Reynolds number (Rodríguez et al., 2015).

The near-wall prism layer parameters used throughout this study are shown in Table 1. The y^+ value of the first cell is kept below 1 for all the simulations, in order to properly resolve the boundary layer. The prism layer is 0.03D in thickness for all the cases with the number of cells in the wall-normal direction given in Table 1. The circumferential number of cells was controlled by two parameters - a target size for the cylinder surface that maintained a reasonable length in wall units in the boundary layer and the target size of the near wall refinement zone. This meant the prism layer was refined in the turbulent zones

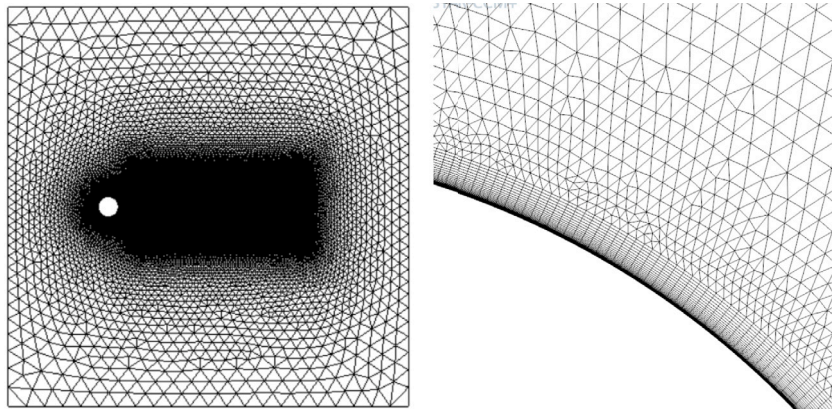


Fig. 2. Left: 2D cut of the square numerical domain showing cylinder centred at $(x, y) = (5D, 10D)$. Right: 2D cut of the near-wall zone of mesh used for the simulations indicating a combination of near-wall prism layer with triangular prisms.

and in the areas of separation and transition, including the free shear layer. The nested zones of refinement had associated target size values getting coarser downstream. For a length preceding the outlet the mesh is coarsened significantly to prevent resolved structures impacting the outlet. The generated 2D plane mesh was then extruded out equally with 94 or 72 cells in the spanwise direction depending on the Reynolds number. An example of the inner zone of one of the meshes can be seen in Fig. 2 (right).

2.4. Boundary/initial conditions and statistic collection

For the boundary conditions, the inlet is a fixed uniform velocity in the streamwise direction necessary to give the correct Reynolds number based on the cylinder diameter and fluid viscosity. Here the cylinder diameter $D = 1$, inlet velocity $U_\infty = 1$ and $\nu = 1/Re$, with no inlet turbulence. For the hybrid and URANS cases the field is initialised using results from a prior RANS simulation. In the spanwise direction a periodic boundary condition is used to mitigate effects associated with the aspect ratio (L_z/D) choice. Symmetry planes are used in the vertical direction at the top and bottom of the computational domain. Finally, for the outlet boundary condition in the streamwise direction, the pressure value and velocity values are extrapolated from the inner cell adjacent to the boundary. To achieve good convergence of the time-averaged statistics the simulation must be performed over many vortex cycles, as discussed in Parnaudeau et al. (2008). For this study, the simulations are performed for an initialisation period after which the statistics are collected at each time step for at least 25 vortex shedding cycles and averaged in the spanwise direction to increase the convergence of the statistics.

3. Results

3.1. Initial study at $Re 2.5 \times 10^5$

We will first give an examination of the SRH model behaviour at the lowest Reynolds number considered, with a particular emphasis on the variation of the SRH model parameters as the grid resolution varies. Table 2 shows a summary of the numerical results for the SRH Lag EB $k - \epsilon$ model compared to the WALE results on the same grids and the high resolution LES. There are two points of immediate interest to consider. Firstly, how does the SRH compare over a range of resolutions to the LES, with the expectation that it performs better owing to its superior ability to adapt to variations in modelled and resolved conditions. Secondly, in the limit as the resolution increases does the SRH method approach essentially LES quality results, the limitations imposed by the shielding in the near wall region notwithstanding. We can also briefly consider the computational saving available in choosing the SRH method over LES.

Table 2

Mean force parameters at Reynolds 2.5×10^5 with reference LES data from Rodríguez et al. (2015). C_D , C_L , mean drag and lift coefficient; $C_{D,rms}$, $C_{L,rms}$ mean fluctuation of drag and lift; $-C_{p,b}$ negative of mean base pressure.

Mesh	CASE	C_D	$C_{D,rms}$	C_L	$C_{L,rms}$	$-C_{p,b}$
A	SRH	0.743	0.052	0.822	0.238	0.73
	WALE	1.247	0.021	0.234	0.008	0.55
B	SRH	0.781	0.066	0.857	0.311	0.80
	WALE	0.896	0.074	0.759	0.401	0.81
C	SRH	0.791	0.073	0.877	0.339	0.82
	WALE	0.812	0.088	0.890	0.491	0.90
	Ref. LES	0.833	0.095	-0.903	0.486	0.99

The first of these points we can approach broadly by considering the summary of the results available in Table 2. We see that on the lower resolution mesh A the SRH model performs substantially better in predicting the time-mean drag, where the LES over-predicts.

The second broad point was how closely the SRH comes to approximate LES quality results as the resolution increases, that is, outside of the shielded region which will produce close to RANS solutions. Again, we can make an initial consideration simply by comparing the integral quantities on the highest resolution grid C and the reference LES data. The results for the all three data sets are in close agreement for the first-order quantities, time-mean drag and lift. Owing to the use of the URANS in the near-wall region, dampening any resolved turbulent structures, the magnitude of the force fluctuations is attenuated by the SRH model which represents the most substantial difference between the LES and SRH results.

We can also now briefly consider the capacity of the SRH model to accurately capture higher-order statistics when compared to resolved LES, and how the grey-area may affect this. Fig. 3 shows a comparison of the predicted cross-stress $\overline{u'v'}$, a significant stress in the breakdown mechanics of the shear layer, between the SRH model on the coarse grid A and the LES on the most refined grid C. Qualitatively there is broad agreement in the distribution of the stress with some variation in the magnitude of the stress predicted. In particular, the SRH seems to predict smaller magnitudes of the stress in the lower shear layer. Both produce an asymmetrical distribution, the bottom shear layer showing 3 times greater magnitude than the upper, owing to the single-bubble regime observed at Reynolds 2.5×10^5 .

Lastly, we consider the cost-saving represented by use of the SRH method. It is impossible to give any precise value given the limitations of the information as available — lack of computational cost data from the reference studies and variation of results with time-step being the two greatest omissions. Nonetheless, by noting that the SRH results on grid A are comparable to the LES results on grid C or B and taking the

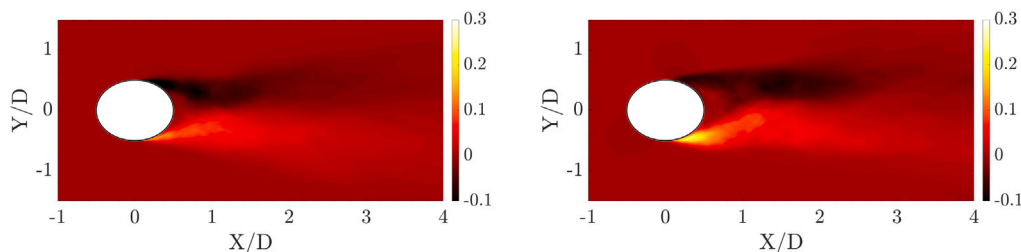


Fig. 3. Resolved Reynolds stress $\overline{u'v'}$ at $Re 2.5 \times 10^5$ for (left) SRH model and (right) WALE on grid C.

Table 3

Details of computational cost at different Reynolds numbers. N_{total} , total number of cells in the grid; $N_{cell,ref}$, number of cells in the corresponding grid from the Rodríguez et al. (2015) study; CPU, average CPU time in hours for simulation run at Re number 2.5×10^5 .

Grid	N_{total}	$N_{cell,ref}$	Model	CPU (hrs)
A	7.65mil	38.4mil	SRH	4695
			WALEs	4455
B	9.72mil	48.6mil	SRH	9605
			WALEs	9270
C	12.43mil	64.1mil	SRH	13715
			WALEs	12150
D	16.64mil	89.4mil	SRH	–

ratio of the approximate CPU time cost on each grid shown in Table 3 for the SRH and LES methods respectively we can say that for the lowest Re number the cost in this case was approximately 39% of the WALEs on the C grid and 51% compared to WALEs on the B grid. All the cases were run on a cluster consisting of nodes of 2 x 20 core Intel Xeon Gold 6248s operating at 2.50 GHz with Infiniband interconnection. The computational saving generated by the reduction in the required resolution is far greater than the slight increase in cost represented by the extra transport equations to be solved. The large bulk of this saving comes from being able to achieve accurate results from a much smaller time step since the Grid A time-step is half that of Grid C's.

3.1.1. Hybrid behaviour

We now turn to a more detailed consideration of the hybrid behaviour of the SRH model. It is desirable to confirm certain behaviours we would like to see exhibited by the SRH model, namely: (1) as the grid is refined, does the SRH measured resolved kinetic energy increase, while the total energy remains approximately constant?, and (2) how does the URANS-LES transition varies as the resolution changes, and how does this affect the grey area?

Fig. 4 shows the long time-averaged values of the ratio of resolved-to-total turbulent kinetic energy k_r/k_t and the total turbulent kinetic energy k_t on the centreplane at Reynolds 2.5×10^5 . Clearly on Grid A the resolution is sufficient for the SRH model to resolve a large amount of the turbulent kinetic energy, with values over 70% for k_r/k_t in most of the domain. Nonetheless, as the resolution is increased the measured proportion of resolved turbulent kinetic energy increases in kind — the desirable behaviour we expect. This is accompanied by a slight decline in the total turbulent kinetic energy as we can see in the rest of the figure. This suggests, at least qualitatively, that the model is adjusting the amount of introduced or modelled turbulent kinetic energy down as the grid refinement increasingly supports higher resolution.

The second of these queries, namely the overall hybrid behaviour and variation of the model parameters requires detailed consideration of the extent of the shielding zones and the location and thickness of the grey-area. Fig. 5 (left) shows the time-mean extent of the shielded region around the cylinder edge for the two grids A and C by plotting the isoline of $f_s = 0.01$. We see that, with a small degree of variation, the extent of the shielded region is consistent between the grids and consistent around the cylinder after approximately 90 deg. In both

cases this shield front lies within the boundary layer, which is to be expected given the shielding function was calibrated to fall away at $y = 100$ in channel flow. Fig. 5 (right) indicates the location and approximate size of the grey-area by plotting isolines of the SRH Energy ratio function at 0.99 and 0.2 (assuming 80% resolution equates to LES) for the grids A and C. Again, we see that similar to the shielding equation the transition zone is relatively invariant to the grid resolution. The inner edge of the grey-area is here mostly determined by the shielding function so the invariance of that function produces a stability for the grey-area across the grids. The outer edge shows more substantial variation. The grey-area on grid C is both closer to the wall and narrower reflecting the greater resolution sustained by the grid. The grey-area itself remains relatively narrow (approximately $0.05D$ for grid A) though it does intersect directly with the area of the free shear layer and therefore likely has a significant effect on the separation dynamics.

As to the question of whether the shielding provided is sufficient, there is reason to believe that, though in this case there is no substantial deleterious effect on the overall results, the shielding is unlikely to be optimal for a large range of cases. Previous studies have for instance already noted the presence of a log-layer mismatch in a channel flow set-up (Manceau, 2018). Different opinions exist in the literature regarding appropriate shielding with some advocating, including in the original conception of DES, for the total shielding of the boundary layer, while some argue that the outer boundary layer should be resolved if the spatial resolution is sufficient. Here the intention of the shielding to extend to $y^+ = 100$ puts the shielding method firmly in the latter category. Allowing the LES mode nearer to the wall can permit the rapid development of unsteady structures but can also lead to a log-layer mismatch. In this case the thinner shielding is necessary for capturing the breakdown of the shear layers that would otherwise be stabilised if shielded. Finding an ideal shielding remains a challenging problem and it is likely that there is no ideal universal shielding function.

3.2. Varying Reynolds numbers

3.2.1. URANS method

Firstly, an examination is made of the results of the URANS cases run using the Lag EB $k-\epsilon$ model. Previous numerical studies both by the authors (Mays et al., 2021) and in various studies from the literature have found that linear eddy-viscosity models (LEVMs) are generally unable to accurately capture the relevant flow physics, with mixed results for Reynolds Stress Models (RSMs) (Palkin et al., 2016). Given that the formulation of the SRH model provides a smooth transition between pure RANS behaviour and LES/DNS behaviour with increasing temporal and spatial resolution, URANS cases using the same basis model provide a baseline case for comparison with later hybrid results. It also represents the still ubiquitous method used in industry for flows of practical relevance.

It is clear from the C_D values in Table 4 and the predicted C_p distributions around the cylinder surface, seen in Fig. 6, that the RANS formulation is not capable of matching the experimental reference data. The failure in these cases is due to the inability of the RANS model to

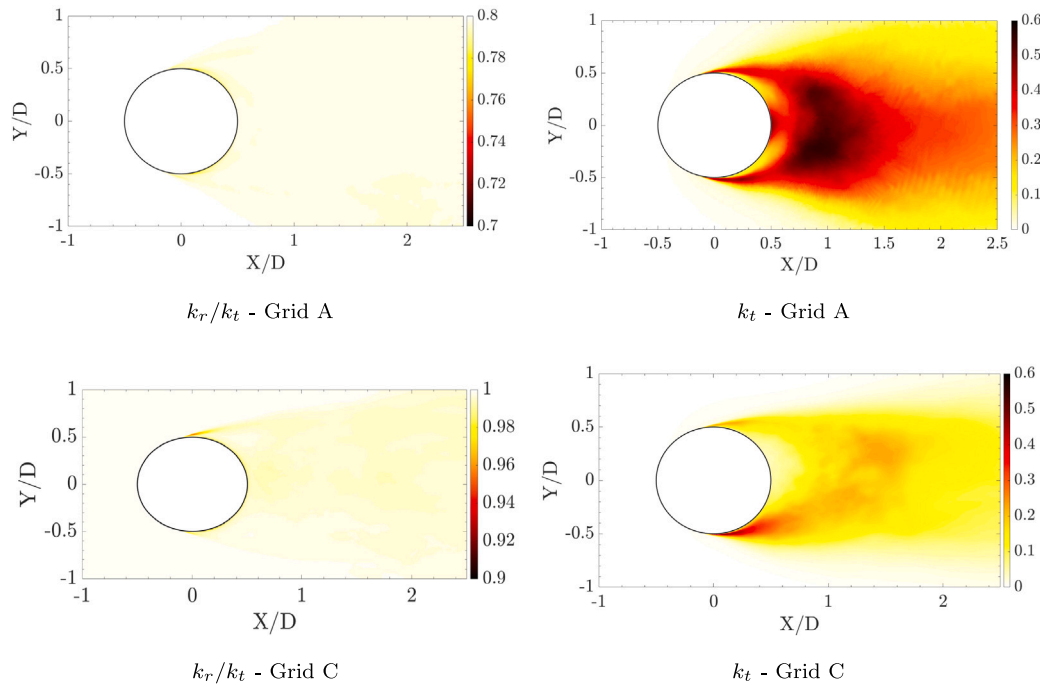


Fig. 4. Long time-averaged (Left) resolved-to-total turbulent kinetic energy k_r/k_t and (Right) normalised total turbulent kinetic energy k_t/U_∞^2 fields for the A and C grids on the centreplane of the computational domain in the spanwise direction.

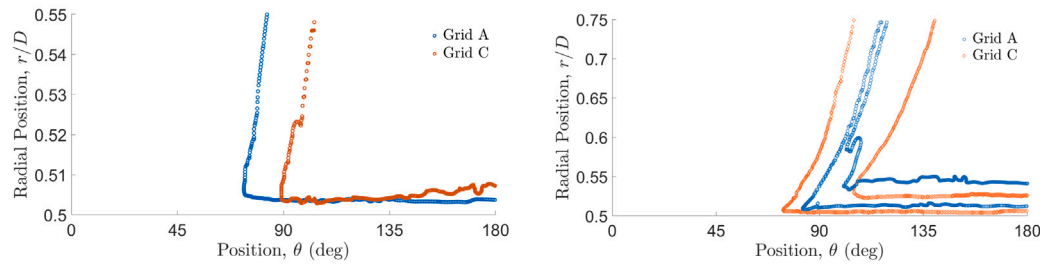


Fig. 5. Variation of hybrid parameters at $Re\ 2.5 \times 10^5$ on three grids: (left) location of shield front ($f_s = 0.01$) and (right) location of grey area boundaries.

Table 4

Mean force parameters for different Reynolds numbers (grid indicated in brackets) with reference LES data from Rodríguez et al. (2015). C_D , C_L , mean drag and lift coefficient; $C_{D,rms}$, $C_{L,rms}$ mean fluctuation of drag and lift; $-C_{p,b}$ negative of mean base pressure. Cases with * chosen as representative SRH case for discussion of results.

Re	CASE	C_D	$C_{D,rms}$	C_L	$C_{L,rms}$	$-C_{p,b}$
2.5×10^5	URANS (A)	0.436	0.023	0.102	0.187	0.95
	*SRH (A)	0.743	0.052	0.822	0.238	0.73
	SRH (B)	0.781	0.066	0.857	0.311	0.80
	Ref. LES	0.833	0.095	-0.903	0.486	0.99
3.8×10^5	URANS (B)	0.354	0.005	0.082	0.082	0.94
	*SRH (B)	0.456	0.042	0.144	0.159	0.39
	SRH (C)	0.475	0.044	0.206	0.188	0.43
	Ref. LES	0.481	0.061	0.245	0.217	0.48
5.3×10^5	URANS (C)	0.204	0.013	0.0054	0.0396	0.95
	*SRH (C)	0.252	0.015	0.0264	0.0569	0.35
	SRH (D)	0.292	0.013	0.0321	0.0628	0.31
	Ref. LES	0.296	0.011	0.0614	0.0705	0.305
7.2×10^5	URANS (D)	0.156	0.0041	0.005	0.0294	0.93
	SRH (C)	0.301	0.0075	-0.011	0.0365	0.44
	*SRH (D)	0.276	0.0068	-0.008	0.0552	0.31
	Ref. LES	0.213	0.0094	0.016	0.0752	0.224

adequately capture the onset and development of the free shear layer breakdown. The work by Pereira et al. (2019) provides a condition on the required effective Reynolds number, effectively the inverse of

turbulent or sub-grid viscosity, in the vicinity of the free shear-layer necessary to observe the correct breakdown behaviour. This indicates that the RANS model is over-predicting the turbulent viscosity. The high levels of turbulent viscosity in the shear layers cause the shear layers to remain stable. This is consistent with previous studies based on linear-eddy viscosity URANS models for a similar test case (Palkin et al., 2016).

The presence of a slight inflection point around the point of separation, similar to the one observed in the present SRH and reference LES data, as well as a non-zero magnitude for the time mean lift coefficient indicates that the model does capture the laminar separation bubble to a certain extent. The model is, however, not capable of adequately predicting fluctuating force data and the re-circulation bubble is overly broad and long when compared with WALE reference LES results, as seen in Table 5.

3.2.2. Hybrid RANS/LES: SRH model

Hybrid RANS/LES closure models are the most novel methods for treating this type of separated flows around a bluff body, and they have the potential to provide near LES performance on a RANS-type mesh. Here we consider the results from the novel SRH model used with the hybrid convective scheme discussed in Section 2.2 with $\sigma = 0.01$ for the BCD scheme used in the LES-like zones.

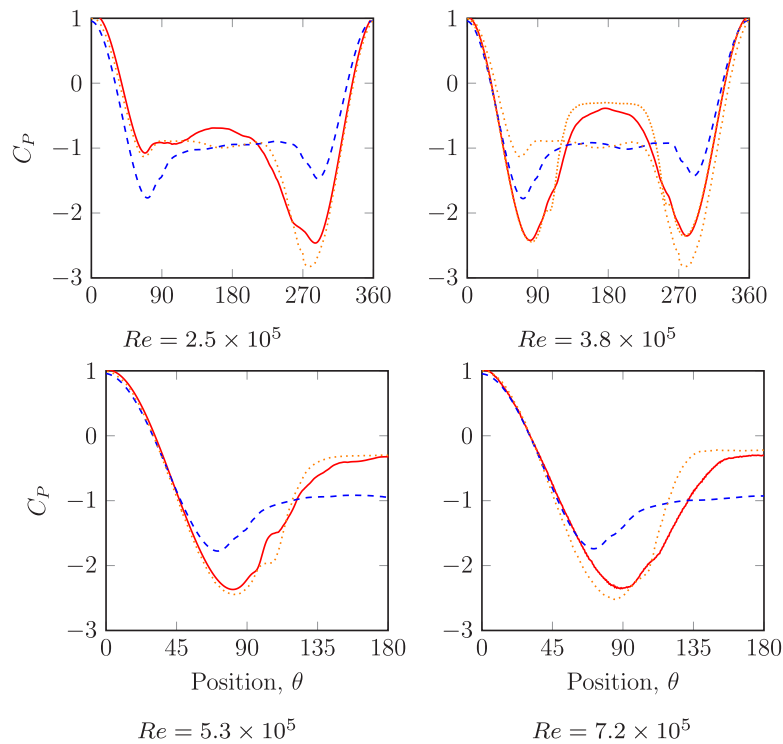


Fig. 6. Mean pressure coefficient profiles around cylinder wall for different Reynolds numbers. Solid line (—) indicates the SRH case with asterisk in Table 4, dashed line (---) indicates the URANS case and dotted line (·····) the reference LES. At $Re = 3.8 \times 10^5$ the reference LES data is for $Re = 2.5 \times 10^5$ (·····) and 5.3×10^5 (·····).

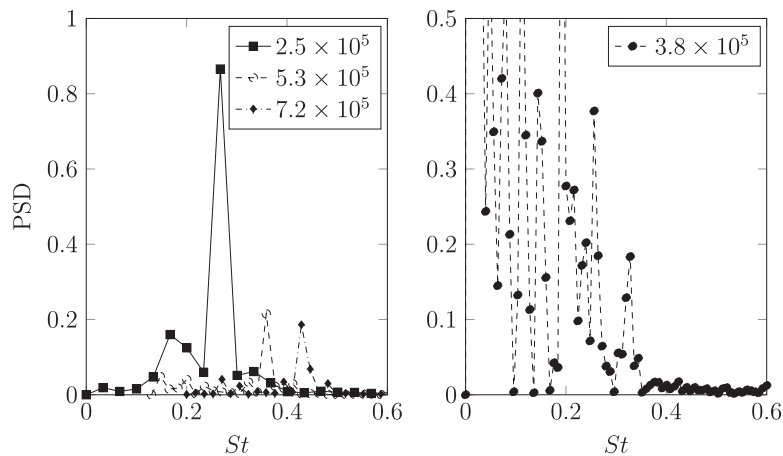


Fig. 7. Power spectral density (PSD) of the fluctuating lift for representative SRH cases at different Reynolds numbers.

Force results and flow topology. A *prima facie* consideration of the predicted mean force values suggests that the SRH model has performed well. Looking at the C_D results in Table 4, which are also shown graphically in Fig. 1, there is a strong agreement with the reference LES and experimental data. However, given the dominance of pressure-drag for separated bluff-body flows, an accurate prediction of the back pressure and overall profile of the pressure coefficient is sufficient to give accurate drag values. This does not guarantee that more complicated flow phenomena like the formation of laminar separation bubbles and the asymmetric flow configurations identified by Rodríguez et al. (2015) are captured properly. Assessment of the presence of these features requires consideration of the existence of precise inflections in the C_p profiles. Nonetheless, the overall trend of the pressure distribution is well captured here — the highly asymmetric profile for a Reynolds number of 250,000 indicates that the one bubble flow condition is captured and the profiles move back towards symmetry as the flow enters into the super-critical regime. The two highest

Reynolds number cases have almost identical profiles in line with the observations of Rodríguez et al. (2015), with the super-critical regime being substantially less sensitive to the Reynolds number.

In this case, the lift coefficient also matches fairly well the reference data, though not as closely. The correct prediction of the lift coefficient requires an accurate determination of the strength and angular size of the laminar separation bubble(s) (LSB). By looking at the pressure coefficient profiles for different critical Reynolds numbers in Fig. 6 ($Re = 2.5 \times 10^5$ and $Re = 3.8 \times 10^5$), the agreement between the reference and the SRH results is not as good around the plateau which is indicative of the LSB. Small variations in the predicted point of initial separation and subsequent reattachment, which are highly sensitive to the model formulation, are essentially responsible for this disagreement. Regardless, the agreement is still fairly strong for the mean quantities.

Regarding the forces fluctuations, the agreement with the reference LES is not as good. As previously discussed and also demonstrated in

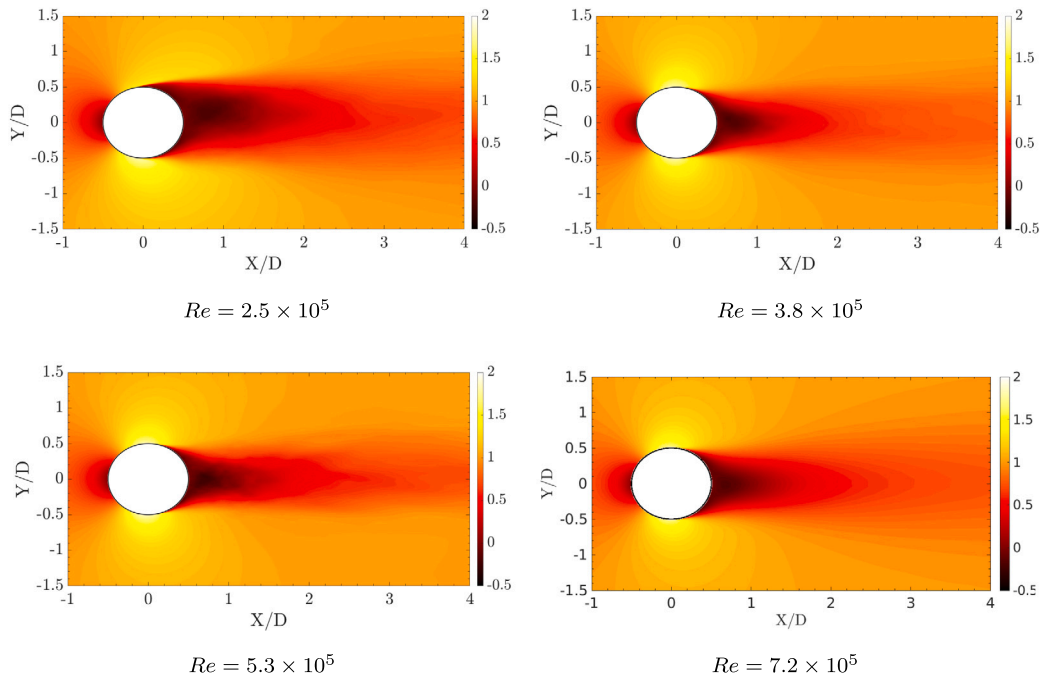


Fig. 8. Time-averaged normalised-streamwise velocity \bar{U}/U_∞ fields for different Reynolds numbers on a 2D plane in the middle of the computational domain in the spanwise direction.

Table 5

Flow parameters for different Reynolds numbers (grid indicated in brackets) with reference LES data from Rodríguez et al. (2015). L_r , mean recirculation bubble length; ϕ_{sep} , mean separation point; St , Strouhal number.

Re	CASE	L_r (m)	ϕ_{sep} (deg)	St
2.5×10^5	URANS (A)	1.107	132	0.35
	SRH (A)	0.611	88/215	0.24
	Ref. LES	0.559	90/218	0.25
3.8×10^5	URANS (B)	1.311	156	0.40
	SRH (B)	0.603	130	0.28
	Ref. LES	0.641	134	0.23
5.3×10^5	URANS (C)	1.339	159	0.43
	SRH (C)	0.676	135	0.35
	Ref. LES	0.727	142	0.38
7.2×10^5	URANS (D)	1.184	157	0.52
	SRH (D)	0.595	155	0.43
	Ref. LES	0.569	148	0.45

Fig. 1, there is a substantial scattering of the experimental data for the force coefficients, both in the mean value and the magnitude of the fluctuations, which is a product of both the difficulty to capture these quantities experimentally but also a reflection of the sensitivity of the forces to different flow conditions. However, the under-prediction of the magnitude of the fluctuations in the present work is perhaps attributable to the dampening effect of the essentially URANS near-wall behaviour. Nonetheless, the disagreement between the reference and the SRH model are not substantial and represent a significant improvement over URANS methods.

Other features of the flow field also suggest the overall good performance of the SRH model. The vortex shedding mechanism appears to be well captured with the Strouhal number in good agreement with the reference values. This is reflected in the very similar profile for the power spectral densities (PSD) of the lift, as seen in Fig. 7, when compared with those reported in Rodríguez et al. (2015). The topological features of the wake are similar also with good agreement for the length of the re-circulation bubble, L_r and the appropriate narrowing of the wake with increasing Reynolds number is clearly visible in Fig. 8.

As discussed in the introduction, the reference LES study found that at Reynolds 2.5×10^5 the flow exhibits an asymmetric single separation bubble state. The existence of a bubble on only one side of the cylinder lead to a significant non-zero value for the lift coefficient and strong asymmetry in the velocity field. This is consistent with our results which shows a strong upward deflection of the recirculation bubble and a positive value for the lift coefficient one order of magnitude greater than at other Reynolds numbers.

Model qualitative behaviour. Having established the good performance of the SRH model in quantitative terms, we now consider the qualitative behaviour of the model and the influence of the parameters controlling the model. We first focus on the questions raised by Heinz (2020) for hybrid models. In particular, we can check whether the model has “an appropriate response [...] to mesh-implied resolution changes” which raises issues relating to the measurement and prediction of the resolved and modelled turbulent kinetic energy contributions.

A major indicator of the effect of the hybridisation in SRH model as compared with the URANS is the SRH correction factor, ψ_H , with an instantaneous example of a distribution for $Re = 3.8 \times 10^5$ shown in Fig. 9. The absolute values of the function alone cannot reveal anything meaningful except in comparison with cases using the same base RANS model. However, the qualitative distribution of ψ_H is as expected with areas of local maximum in the wake and shear layers, i.e. areas of strong turbulence away from the immediate vicinity of the wall, whereas regions of no turbulence or very near-wall take a value of 1 ensuring a URANS behaviour. The rapid development of values greater than 1 when moving from the wall to the free stream is critical to mitigate grey-area effects and here indicates a robust behaviour necessary for correctly capturing the Kelvin–Helmholtz breakdown.

Fig. 10(a) also indicates the behaviour of the shielding function. We see that the function provides shielding in the expected areas near the wall while allowing the shear layer to be fully resolved. The shielding also extends upstream of the cylinder, which is perhaps unintended, as a result of low levels of turbulence, but with no detrimental effect given the fully laminar nature of the flow in this region. As noted in a previous study (Mays et al., 2021), the form of the shielding function (Eq. (13)) is identical to that of a DDES but the DDES shielded zone

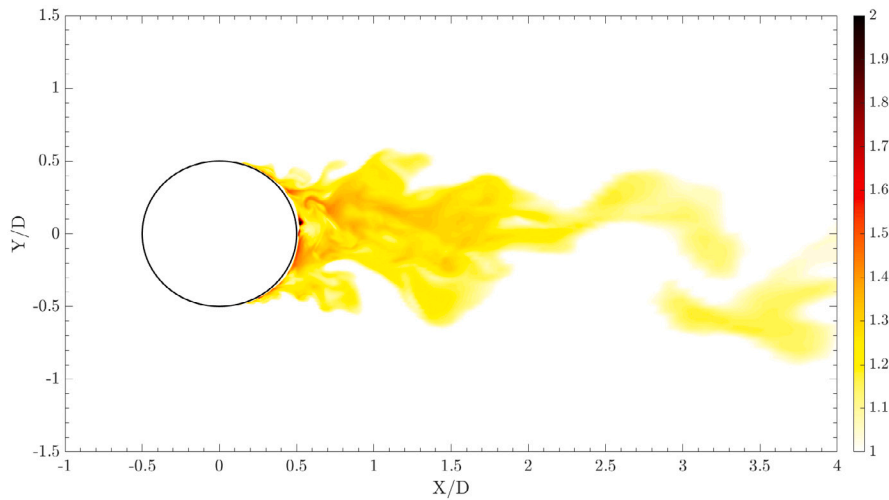


Fig. 9. Instantaneous SRH correction factor ψ at $Re = 3.8 \times 10^5$.

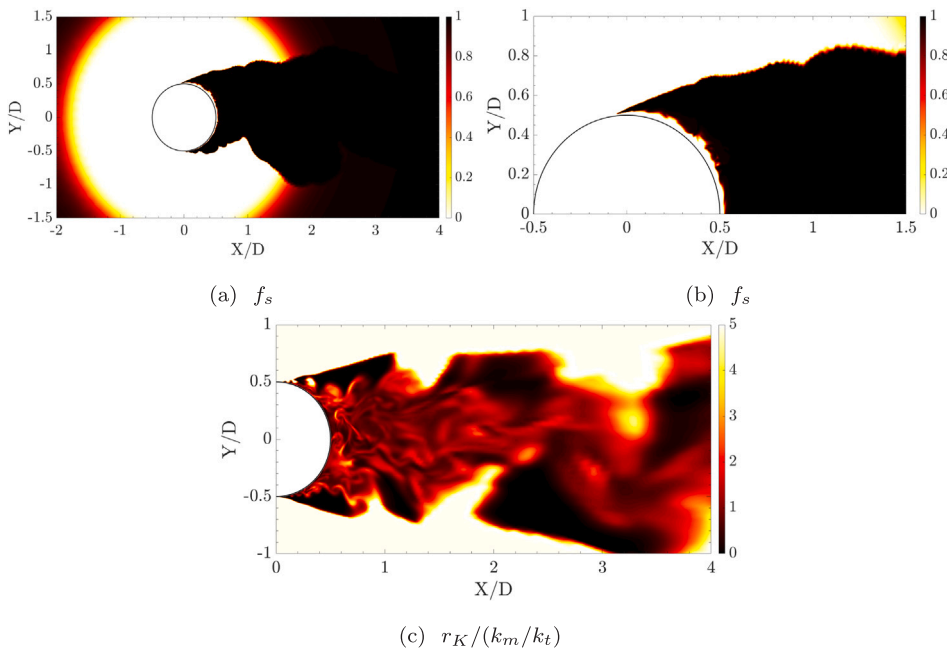


Fig. 10. Shielding function, f_s and ratio of theoretical-to-realised energy ratio at Reynolds number 3.8×10^5 . The distributions shown in the figure are typical for all Reynolds numbers examined in the present study.

is generally much broader, producing a RANS-like solution. The difference in behaviour can only be attributed to differences in the model formulation, which does suggest that the SRH model is more sensitive and the formation of unsteady content is more easily triggered, an ideal behaviour that reduces the necessary initialisation period. However, while the SRH model does not display the typical grey-area effect of a very slow transition in turbulent viscosity, the authors of the original formulation of the SRH model (Manceau, 2018) have noted that the shielding in other cases can be insufficient such as in channel flows where it produces a significant log-layer mismatch. This causes errors both in the velocity at the edge of the boundary layer and in the wall shear stress. Regardless, given the success of the results it seems that the ability to rapidly form unsteady content and capture the correct shear-layer breakdown is more important in these cases.

A major question raised by Heinz (2020) in the context of hybrid model behaviour is the use of a parameter to drive the theoretical partition of energy, here r_K , and whether it then matches the partition observed in the simulation. In Fig. 10(c) we see the ratio of r_K to

the realised energy ratio as measured by the SRH model using an exponential averaging. We can see that in the majority of the regions dominated by turbulent motions there is an approximate agreement between the predicted and realised energy ratios. Areas that are weakly turbulent or essentially irrotational diverge more from unity due to the invalidity of the assumption of an Euler spectrum of turbulence underlying the definition of r_K . Nonetheless, the generally good agreement in the appropriate zones suggests that using the r_k function to control the hybridisation works adequately, though there may be room for improvement.

The maximal values of the sub-grid viscosity for the SRH cases can be seen in Table 6. These are substantially lower compared with the URANS simulations, which are typically on the order of ten times greater at least. As a result, instabilities can develop early in the shear layer and the breakdown mechanism of the shear layer is then simulated accurately. The qualitative distribution of the sub-grid viscosity in Fig. 11 for the SRH model is also as desired with the maximal values dispersed throughout the far wake, initially increasing as the

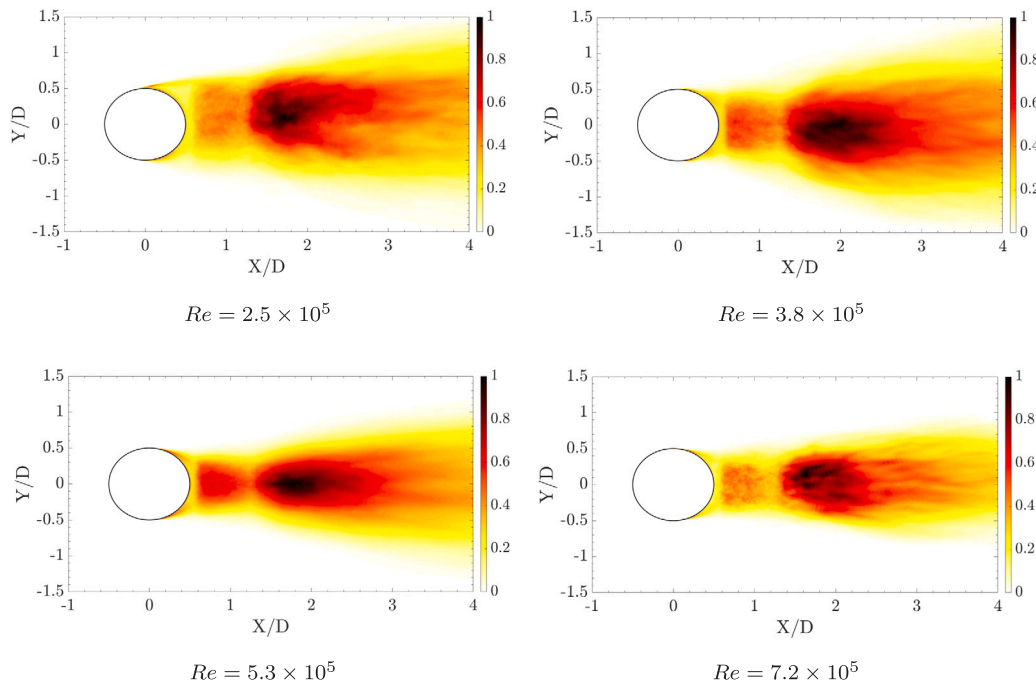


Fig. 11. Time-averaged sub-grid viscosity ratio v_{sgs}/ν fields normalised by their respective maximum values as seen in Table 6 for different Reynolds numbers.

Table 6

Maximum values of the sub-grid viscosity ratio v_{sgs}/ν for different Reynolds numbers.

Re	2.5×10^5	3.8×10^5	5.3×10^5	7.8×10^5
v_{sgs}/ν	9.4	9.8	14.5	18.3

mesh coarsens downstream and then decreasing again as the turbulence dissipates. Overall, this indicates an excellent behaviour for the SRH model which is free of issues with premature transition and shows a good ability to resolve unsteady structures, as in the LES reference data.

The shear layer breakdown observed in Fig. 12 for the Lag EB $k - \epsilon$ model is qualitatively similar to the one observed in the high-resolution WALE LES case. The structures display a degree of stratification in the spanwise direction but this is attributable to the coarsening of the spanwise resolution and does not appear to have any significant impact on the results.

The Lag EB $k - \epsilon$ SRH implementation is highly convenient as the underlying RANS formulation provides the improvement in the prediction of transition, separation and non-linear effects without the use of ad-hoc transition models. However, in addition to potential issues with grey area effects and insufficient shielding (Duffal et al., 2019), the interaction between the SRH modifications and the base RANS model produces a spurious reduction in the reduced stress function in the free stream. When used for channel flow simulations at high Reynolds number, this has caused very poor results by comparison with other methods. Combined, these effects can produce a substantial log-layer mismatch. Nonetheless, the greater importance of very near-wall effects and the dominance of pressure drag in this case means that issues with log-layer mismatch become secondary to the improvements offered by the Lag EB model.

Mesh resolution. We now re-examine a point considered for the results at Reynolds number 2.5×10^5 . One of the major motives behind the development of hybrid RANS/LES models, besides the ability to capture accurate unsteady flow statistics which was discussed and demonstrated in the previous sections, is the potential to reduce mesh resolution, especially in the near-wall region, without substantially affecting accuracy. To that end we now consider the effect of resolution

on the results and also on the savings relative to the reference LES study. Looking at Table 4 we see that in each case moving from the coarser mesh to the more refined brought the results closer to the reference data but the difference between the two meshes used for each Reynolds number is not substantial.

In comparison with the LES reference data all the meshes used here were 5 times smaller at the relevant Reynolds number, see Table 3, and as established that did not prevent near-LES quality results. However, this discussion must be qualified by two points. Firstly, the reference LES case actively sought to resolve most of the scales in the far wake, whereas we have deliberately coarsened this area of the flow. As such, Rodríguez et al. (2015) most likely could have achieved similar quantitative results for the force coefficients at a reduced mesh size if they had so desired, as has been achieved here for the lowest Reynolds number. Secondly, and more importantly given the impetus of hybrid models, is to consider any possible savings in the near-wall region of the mesh. While the exact design of the prism layers in the reference case is not specified, by visually examining the figures provided for the mesh used at Reynolds 530,000 we can estimate that the circumferential length of a prism cell was approximately $0.001D$ which is substantially smaller than the cells used here. Such size of cell would also be more in-line with recommendations for LES simulations of turbulent boundary layers (Pope, 2000). This would suggest that the SRH model does indeed provide an opportunity for a reduction in computational cost. Overall, for robustness, convenience and low computational cost the Lag EB $k - \epsilon$ SRH model appears to be a strong choice for simulating highly-separated external flows at high Reynolds numbers.

We have already considered the r_k function in the context of Heinz (2020) questions and whether it is accurately determined. Now, we can consider this again but specifically in the context of a measure of mesh resolution. While the energy ratio does seem to be generally accurately predicted by r_k , in essentially turbulence free areas r_k is more varying value since it is not well defined any more. On the other hand, using the determined energy ratio, such as is seen in Fig. 13 for Reynolds 720,000 on the coarser mesh, this can accurately highlight areas of insufficient resolution. In this example, we can see a patch with approximately 40% modelled contribution which may not be sufficient for accurate results. However, it must be said this can only be done *a posteriori*

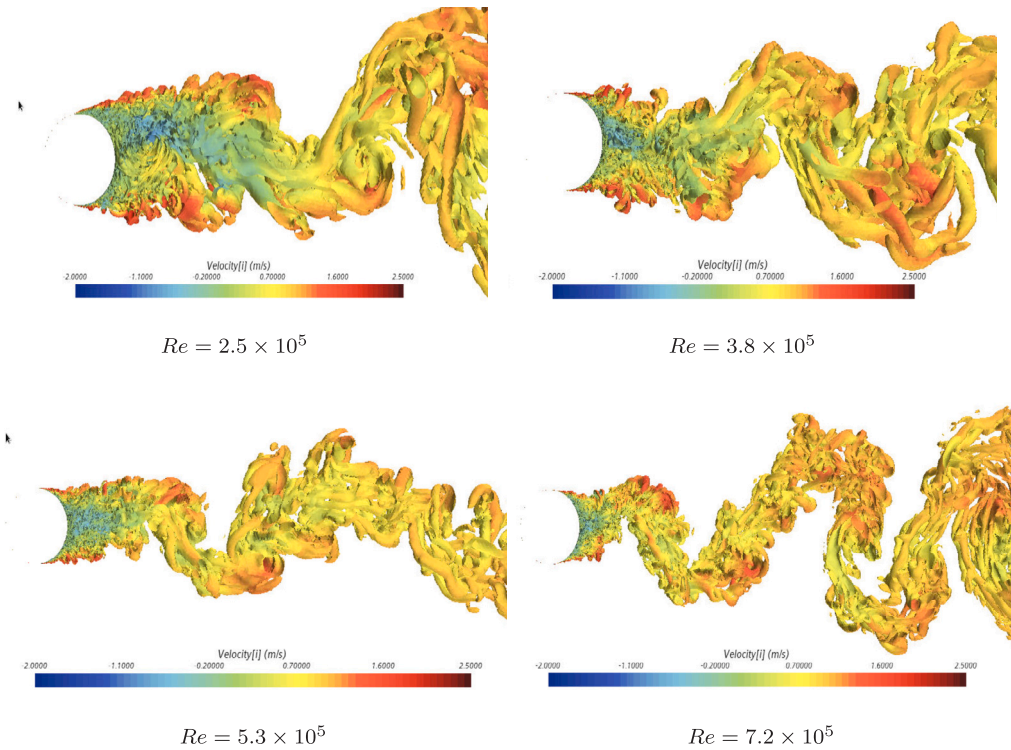


Fig. 12. Iso-surfaces of instantaneous realisation of Q-criterion ($Q = 0.5$) coloured by streamwise velocity for different Reynolds numbers.

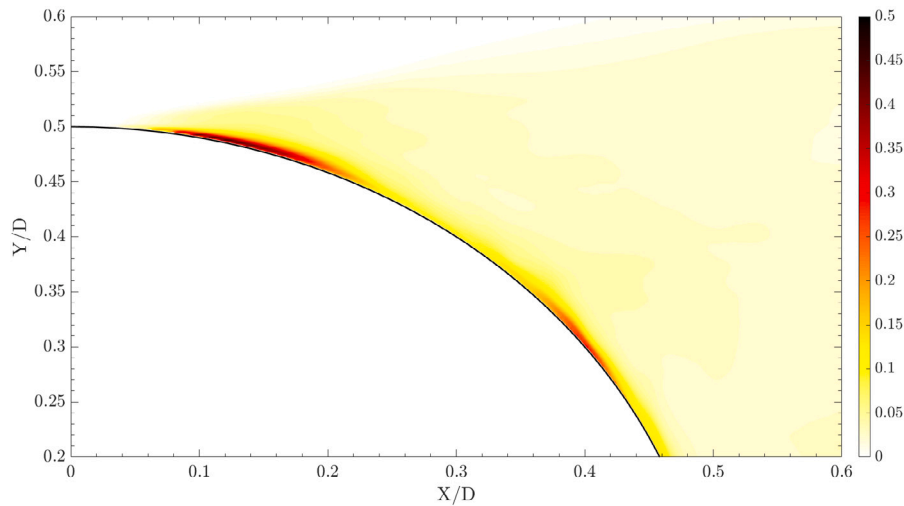


Fig. 13. Ratio of mean modelled to mean total turbulent kinetic energy at $Re = 7.2 \times 10^5$.

and will be only approximately correct after the initialisation period. Counter to that, using r_K as a simple measure with RANS initialisation conditions provides a simple *a priori* measure, with a reasonable degree of accuracy.

4. Conclusion

Simulations of the flow over a smooth cylinder using a novel scale-resolving hybrid method with the Lag Elliptic Blending $k - \epsilon$ RANS model as a basis, have been performed for Reynolds numbers in the critical and super-critical regimes. In general the results are good with particularly strong agreement between the reference data for the mean force values, although more precise features of the flow field such as the size of the laminar separation bubbles are not so easily found. The predicted Strouhal number and power spectra based on the lift also

agrees quite well suggesting that the underlying physics of the shear-layer breakdown and vortex shedding are well captured. On the other hand, the magnitude of the RMS fluctuations of drag and lift are not so closely in agreement with the reference data, although this can largely be attributed to a dampening effect of the RANS model near to the wall. Nonetheless, fluctuations of moderate value exist and are significantly improved over pure URANS.

The qualitative behaviour of the SRH model is also as desired. The shielding function enforces the RANS behaviour in all of the near-wall region but is both thin and permits the shear-layer to rapidly break down. The corrective factor ψ_H is concentrated in the shear layers and wake particularly in the fine areas of the mesh. Despite detrimental effects of the SRH modification interacting with the reduced stress function transport equation and potential issues with log-layer mismatch,

overall the combined SRH Lag EB $k - \epsilon$ accurately captures complex physical behaviours.

One point that has not been explored in this study is the potential for significantly coarsening the time step without major impact on the results. The formal derivation of the model theoretically allows for smooth variation of the split between the modelled and resolved turbulent kinetic energies as spatio-temporal resolution varies, and so one expects to see robust behaviour of the model with regard to varying time-step. This is a key point to explore in subsequent studies. On this point, it should be noted that most of the published works do not provide explicitly the values of the time steps used for the simulations. It is expected that the SRH approach would allow for much larger time steps than LES approaches, with great potential to further reduce the cost of simulations.

Mesh resolution requirements near to the cylinder wall remained high since under-resolution is fatal to accurate prediction of transition and separation effects. Regardless, the SRH model permitted a substantial reduction in computational effort by allowing coarsening of the wake with no detrimental effects and also a reduction in the required number of circumferential cells in the prism layers relative to fully resolved LES. Near-LES quality results, therefore, were achieved on meshes 5 times coarser than the reference LES mesh.

CRedit authorship contribution statement

Michael D. Mays: Conceptualisation, Methodology, Validation, Writing – original draft. **Sylvain Lardeau:** Methodology, Software, Writing – review & editing, Resources. **Sylvain Laizet:** Conceptualisation, Writing – review & editing, Supervision.

Declaration of competing interest

The authors declare that they have no known competing financial interests or personal relationships that could have appeared to influence the work reported in this paper.

Data availability

The authors do not have permission to share data.

Acknowledgement

This work was supported by a PhD scholarship funded by EPSRC and Siemens Industry Software SAS, EPSRC ICASE 2018 (EP/S513635/1). For the purpose of open access, the authors have applied a Creative Commons Attribution (CC BY) licence to any Author Accepted Manuscript (AAM) version arising.

Appendix. Lag Elliptic Blending $k - \epsilon P_\varphi$ production term

The precise production term for the reduced stress function is provided for incompressible flow below:

$$P_\varphi = -(2 - C_{\epsilon 1}) \frac{\varphi}{k} P_k + \rho(1 - \alpha^3) f_w + \rho \alpha^3 f_h \quad (16)$$

where f_w the near-wall production source term is

$$f_w = - \left(C_{\epsilon 2} - 1 + 5 - \frac{1}{C_\mu} \right) \frac{\varphi \epsilon}{k} \quad (17)$$

and f_h the homogeneous production source term is

$$f_h = - \frac{\epsilon}{k} \left(C_1 + C_{\epsilon 2} - 2 + C_1^* \frac{P_k}{\rho \epsilon} \right) \varphi + \frac{C_{P3} \epsilon}{k} + \frac{C_3^*}{\sqrt{2}} \varphi S + \frac{\epsilon}{S^2 k} \left[\frac{2}{C_\mu} (1 - C_4) \mathbf{A} \mathbf{S} - \frac{2}{C_\mu} (1 - C_5) \mathbf{A} \widetilde{\mathbf{W}} \right] : \mathbf{S} \quad (18)$$

\mathbf{A} is the Reynolds-stress anisotropy tensor the expression for which is

$$\mathbf{A} = -2 \frac{v_t}{k} \left[\mathbf{S} + \frac{2 - 2C_5}{C_1 + C_1^* + 1} \frac{2}{\sqrt{(\mathbf{S} + \widetilde{\mathbf{W}}) : (\mathbf{S} + \widetilde{\mathbf{W}})}} (\mathbf{S} \widetilde{\mathbf{W}} - \widetilde{\mathbf{W}} \mathbf{S}) \right] \quad (19)$$

where \mathbf{S} is the rate of strain tensor. $\widetilde{\mathbf{W}}$ is the modified absolute vorticity tensor given by:

$$\widetilde{\mathbf{W}} = \widetilde{\mathbf{W}} - \mathbf{W}^s \quad (20)$$

where $\widetilde{\mathbf{W}}$ is the absolute vorticity tensor which for this case, given the lack of frame rotation, is equal to the vorticity tensor and \mathbf{W}^s is the Spalart–Shur tensor given by:

$$\mathbf{W}^s = \frac{1}{S^2} \left(\mathbf{S} \frac{D\mathbf{S}}{Dt} - \frac{D\mathbf{S}}{Dt} \mathbf{S} \right) \quad (21)$$

The various model constants values are found in the STAR-CCM+ documentation (Siemens, 2021).

References

- Achenbach, E., Heinecke, E., 1981. On vortex shedding from smooth and rough cylinders in the range of Reynolds numbers 6×10^3 to 5×10^6 . *J. Fluid Mech.* 109, 239–251. <http://dx.doi.org/10.1017/S002211208100102X>.
- Billard, F., Laurence, D., 2012. A robust $k - \epsilon - v_2/k$ elliptic blending turbulence model applied to near-wall, separated and buoyant flows. *Int. J. Heat Fluid Flow* 33 (1), 45–58.
- Breuer, M., 2000. A challenging test case for large eddy simulation: High Reynolds number circular cylinder flow. *Int. J. Heat Fluid Flow* 21, 648–654. [http://dx.doi.org/10.1016/S0142-727X\(00\)00056-4](http://dx.doi.org/10.1016/S0142-727X(00)00056-4).
- Chaouat, B., 2017. The state of the art of hybrid RANS/LES modeling for the simulation of turbulent flows. *Flow Turbul. Combust.* 99 (2), 279–327. <http://dx.doi.org/10.1007/s10494-017-9828-8>.
- Duffal, V., De Laage de Meux, B., Manceau, R., 2019. Development and validation of a hybrid RANS-LES approach based on temporal filtering. In: ASME-JSME-KSME 2019 8th Joint Fluids Engineering Conference, Vol. 2. AJKFluids 2019, V002T02A053. <http://dx.doi.org/10.1115/AJKFluids2019-4937>.
- Page, A., 1930. The Drag of Circular Cylinders and Spheres at High Values of Reynolds Number. Technical Report, HM Stationery Office.
- Fung, Y.C., 1960. Fluctuating lift and drag acting on a cylinder in a flow at supercritical Reynolds numbers. *J. Aerosp. Sci.* 27, 801–814. <http://dx.doi.org/10.2514/8.8769>.
- Germano, M., Piomelli, U., Moin, P., Cabot, W.H., 1991. A dynamic subgrid-scale eddy viscosity model. *Phys. Fluids A* 3 (7), 1760–1765.
- Girimaji, S.S., 2006. Partially-averaged Navier–Stokes model for turbulence: A Reynolds-averaged Navier–Stokes to direct numerical simulation bridging method. *J. Appl. Mech.* 73 (3), 413. <http://dx.doi.org/10.1115/1.2151207>.
- Gritskevich, M.S., Garbaruk, A.V., Schütze, J., Menter, F.R., 2012. Development of DDES and IDDES formulations for the $k - \omega$ shear stress transport model. *Flow Turbul. Combust.* 88 (3), 431–449.
- Heinz, S., 2020. A review of hybrid RANS-LES methods for turbulent flows: Concepts and applications. *Prog. Aerosp. Sci.* 114, 100597. <http://dx.doi.org/10.1016/j.paerosci.2019.100597>.
- Lardeau, S., Billard, F., 2016. Development of an elliptic-blending lag model for industrial applications. In: 54th AIAA Aerospace Sciences Meeting. p. 1600.
- Lehmkuhl, O., Rodríguez, I., Borrell, R., Chiva, J., Oliva, A., 2014. Unsteady forces on a circular cylinder at critical Reynolds numbers. *Phys. Fluids* 26, 125110. <http://dx.doi.org/10.1063/1.4904415>.
- Manceau, R., 2018. Progress in hybrid temporal LES. In: Progress in Hybrid RANS-LES Modelling. Springer, Cham, pp. 9–25. http://dx.doi.org/10.1007/978-3-319-70031-1_2.
- Mays, M.D., Laizet, S., Lardeau, S., 2021. Performance of various turbulence models for simulating sub-critical high-Reynolds number flows over a smooth cylinder. In: AIAA Aviation and Aeronautics Forum and Exposition. AIAA AVIATION Forum 2021, pp. 1–17. <http://dx.doi.org/10.2514/6.2021-2762>.
- Moussaed, C., Salvetti, M.V., Wornom, S., Koobus, B., Dervieux, A., 2014. Simulation of the flow past a circular cylinder in the supercritical regime by blending RANS and variational-multiscale LES models. *J. Fluids Struct.* 47, 114–123.
- Nicoud, F., Ducros, F., 1999. Subgrid-scale stress modelling based on the square of the velocity gradient tensor. *Flow Turbul. Combust.* 62 (3), 183–200.
- Palkin, E., Mullyadzhonov, R., Hadžiabdić, M., Hanjalić, K., 2016. Scrutinizing URANS in shedding flows: the case of cylinder in cross-flow in the subcritical regime. *Flow Turbul. Combust.* 97 (4), 1017–1046.
- Parnaudeau, P., Carlier, J., Heitz, D., Lamballais, E., 2008. Experimental and numerical studies of the flow over a circular cylinder at Reynolds number 3900. *Phys. Fluids* 20 (8), 085101. <http://dx.doi.org/10.1063/1.2957018>.

- Pereira, F.S., Eça, L., Vaz, G., Girimaji, S.S., 2018. Challenges in scale-resolving simulations of turbulent wake flows with coherent structures. *J. Comput. Phys.* 363, 98–115. <http://dx.doi.org/10.1016/j.jcp.2018.02.038>.
- Pereira, F.S., Eça, L., Vaz, G., Girimaji, S.S., 2019. On the simulation of the flow around a circular cylinder at $Re=140,000$. *Int. J. Heat Fluid Flow* 76, 40–56. <http://dx.doi.org/10.1016/j.ijheatfluidflow.2019.01.007>.
- Pope, S.B., 2000. *Turbulent Flows*. Cambridge University Press.
- Rodríguez, I., Lehmkuhl, O., Chiva, J., Borrell, R., Oliva, A., 2015. On the flow past a circular cylinder from critical to super-critical Reynolds numbers: Wake topology and vortex shedding. *Int. J. Heat Fluid Flow* 55, 91–103. <http://dx.doi.org/10.1016/j.ijheatfluidflow.2015.05.009>.
- Schewe, G., 1983. On the force fluctuations acting on a circular cylinder in crossflow from subcritical up to transcritical Reynolds numbers. *J. Fluid Mech.* 133, 265–285. <http://dx.doi.org/10.1017/S0022112083001913>.
- Schmidt, L.V., 1965. Measurements of fluctuating air loads on a circular cylinder. *J. Aircr.* 2, 49–55. <http://dx.doi.org/10.2514/3.43618>.
- Siemens, 2021. Simcenter Star-CCM+. <https://www.plm.automation.siemens.com/global/en/products/simcenter/STAR-CCM.html>. Documentation.
- Smagorinsky, J., 1963. General circulation experiments with the primitive equations: I. The basic experiment. *Mon. Weather Rev.* 91 (3), 99–164.
- Spalart, P., Jou, W., Strelets, M., Allmaras, S., 1997. Comments on the feasibility of LES for wings and on a hybrid RANS/LES approach. *Adv. DNS/LES 1* (January), 4–8.
- Vaz, G., Wal, R.V.D., Mabilat, C., Gallagher, P., 2007. Viscous flow computations on smooth cylinders a detailed numerical study with validation. In: *Proceedings of the International Conference on Offshore Mechanics and Arctic Engineering*, Vol. 3. OMAE, pp. 849–860. <http://dx.doi.org/10.1115/OMAE2007-29275>.
- Zdravkovich, M.M., 1997. *Flow Around Circular Cylinders*. Oxford University Press.